ARTICLE

doi:10.1038/nature10330

Structure of the membrane domain of respiratory complex I

Rouslan G. Efremov[1]† & Leonid A. Sazanov[1]

Complex I is the first and largest enzyme of the respiratory chain, coupling electron transfer between NADH and ubiquinone to the translocation of four protons across the membrane. It has a central role in cellular energy production and has been implicated in many human neurodegenerative diseases. The L-shaped enzyme consists of hydrophilic and membrane domains. Previously, we determined the structure of the hydrophilic domain. Here we report the crystal structure of the *Escherichia coli* complex I membrane domain at 3.0 Å resolution. It includes six subunits, NuoL, NuoM, NuoN, NuoA, NuoJ and NuoK, with 55 transmembrane helices. The fold of the homologous antiporter-like subunits L, M and N is novel, with two inverted structural repeats of five transmembrane helices arranged, unusually, face-to-back. Each repeat includes a discontinuous transmembrane helix and forms half of a channel across the membrane. A network of conserved polar residues connects the two half-channels, completing the proton translocation pathway. Unexpectedly, lysines rather than carboxylate residues act as the main elements of the proton pump in these subunits. The fourth probable proton-translocation channel is at the interface of subunits N, K, J and A. The structure indicates that proton translocation in complex I, uniquely, involves coordinated conformational changes in six symmetrical structural elements.

Complex I (NADH:ubiquinone oxidoreductase) is one of the largest known membrane proteins. It provides about 40% of the proton flux during proton-motive force generation for the synthesis of ATP by the mitochondrial respiratory chain[1–5]. Many mutations in subunits of complex I have been associated with human neurodegenerative diseases[5,6]. Complex I is a major source of reactive oxygen species in mitochondria: these can damage mitochondrial DNA and are considered to be causative agents in Parkinson's disease[7] and ageing[8]. Mitochondrial complex I consists of 45 subunits (980 kDa in total)[9]. The simpler prokaryotic enzyme usually consists of 14 'core' subunits (about 550 kDa in total) that are conserved from bacteria to humans[1,2,5,10]. It contains equivalent redox components and has a similar L-shaped structure to that of mitochondrial complex I (refs 2, 5, 11). The high degree of sequence conservation of core subunits indicates that the mechanism of complex I is probably the same throughout all species.

The complete atomic structure of this molecular machine is currently unknown. Structures of the *Thermus thermophilus* complex I hydrophilic domain[12,13] have established the electron-transfer pathway from NADH to the primary electron acceptor flavin mononucleotide, and then through seven conserved iron-sulphur clusters to the putative quinone binding site at the interface with the membrane domain (which lacks covalently bound prosthetic groups). The three largest hydrophobic subunits of complex I, NuoL, M and N (*E. coli* nomenclature), are homologous to each other and to Na^+/H^+ antiporter complex (Mrp) subunits[14,15]. They are likely to participate in proton translocation. We previously determined the arrangement of α-helices in the membrane domain of *E. coli* complex I, but the limited resolution (3.9 Å) prevented sequence assignment[11].

Understanding how the transfer of two electrons from NADH to ubiquinone is coupled to the translocation of four protons (the current consensus value) across the membrane remains a major question in complex I research[1–3,5]. 'Direct' (redox-driven) and 'indirect' (conformation-driven) mechanisms have been proposed[2,3,5,16]. Recently published structures revealed an unexpected structural element, helix HL, extending along nearly the entire length of the membrane domain[11,17]: this may act as a connecting element, coordinating conformational changes[11]. A greater understanding requires a knowledge of the atomic structure of the membrane domain.

Structure determination and overall architecture

A new *P*1 crystal form was obtained with protein purified in the detergent cymal-7. After extensive optimization, the diffraction extended to 2.7 Å in the best direction. The crystallized fragment contains six subunits, NuoL, M, N, A, J and K (222 kDa in total), but lacks NuoH, which dissociates readily from the complex[11,18]. Multiwavelength anomalous diffraction (MAD) data sets were collected from SeMet-derivatized protein (Supplementary Table 1). Multi-crystal density averaging and modification led to experimental electron density maps of excellent quality (Supplementary Fig. 1). The model was refined to 3.0 Å resolution with $R = 23.2\%$ and $R_{free} = 28.3\%$ (Supplementary Table 1), and includes 1,952 residues (out of 2,038, Supplementary Table 2). A cymal-7 molecule, fragments of lipid aliphatic chains and several well-ordered internal water molecules are also included.

The model contains 55 transmembrane helices (TMs) (Fig. 1 and Supplementary Movie 1). Subunits NuoA, J and K form an 11-helix bundle near the interface with the hydrophilic domain, and the antiporter-like subunits NuoN, M, and L follow, as proposed earlier[11]. The distal subunit NuoL contains a carboxy-terminal extension that starts with TM15, followed by helix HL and ending with TM16, harboured at the interface with subunits NuoJ, K and N. Sequence conservation is high for the membrane core of all subunits (Supplementary Fig. 3), underlining its functional significance. Helix HL is poorly conserved, as might be expected for a mostly mechanical element, with the exception of residues contacting other subunits

[1]Medical Research Council Mitochondrial Biology Unit, Wellcome Trust/MRC Building, Hills Road, Cambridge CB2 0XY, UK. †Present address: Max-Planck Institute for Molecular Physiology, Otto-Hahn Strasse 11, Dortmund 44227, Germany.

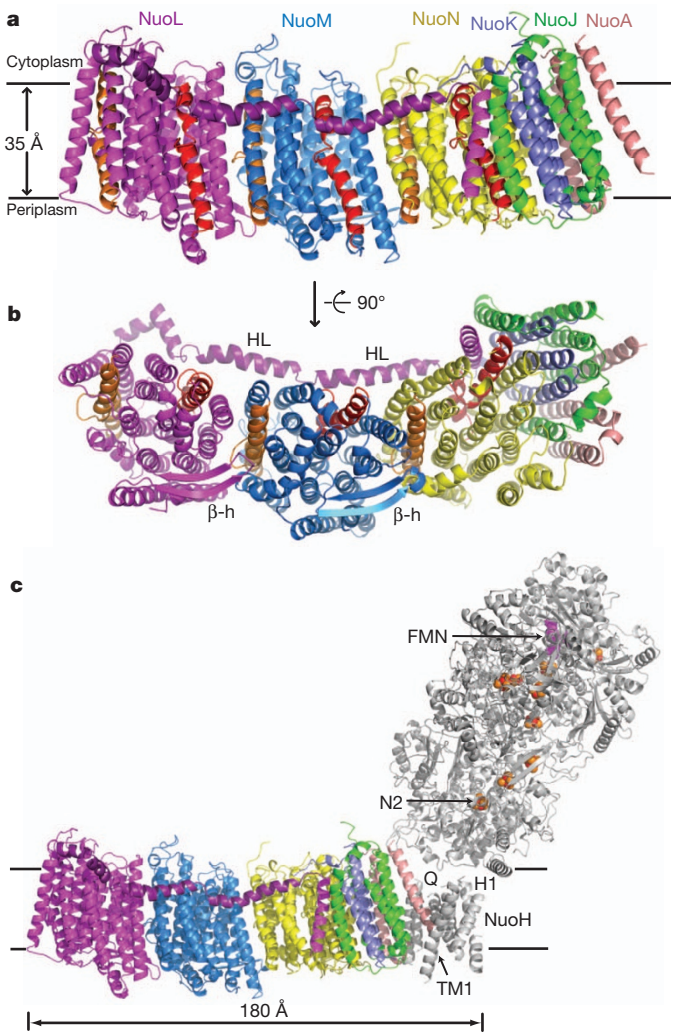

Figure 1 | Architecture of the membrane domain of *E. coli* complex I. Cartoon representation of the atomic model. **a**, Side view in the membrane plane. **b**, View from the periplasm into the membrane. Subunits are coloured as indicated by the labels. Discontinuous helices are shown in red (TM7) and orange (TM12). Connecting elements, helix HL and β-hairpins (β-h), are labelled. The position of the lipid bilayer is estimated as in Supplementary Fig. 4. **c**, Side view of the structure, aligned with the membrane domain of the entire complex I from *T. thermophilus* (PDB code 3M9S)[11]. Subunits that are not present in the *E. coli* structure are shown in grey. Flavin mononucleotide (FMN) is shown as magenta spheres; iron-sulphur clusters are shown as red-orange spheres, with cluster N2 labelled. Helix TM1 from subunit Nqo8/NuoH, helix H1 from Nqo6/NuoB and the probable quinone-binding site (Q) are indicated.

(Supplementary Fig. 3b), indicating that this helix is similarly arranged across species. The polar residues of amphiphatic helix HL face the cytoplasm and apolar residues point to the membrane (Supplementary Fig. 4), indicating that helix HL resides at the surface of the lipid bilayer. The periplasmic surface of the membrane domain is mostly negatively charged and the cytoplasmic surface is positively charged, in agreement with the positive-inside rule[19]. Lipid bilayer boundaries are clearly visualized by the belts of solvent-exposed Tyr and Trp residues[20] and by the hydrophobicity of surface-exposed residues (Supplementary Fig. 4).

Fold of antiporter-like subunits

Subunits NuoL, M and N contain 14 structurally conserved helices (Fig. 2a–c, Supplementary Fig. 5 and Supplementary Table 3). The fold differs from the bioinformatic prediction[21]. Sequential transmembrane helices contact each other, except for TM8 and TM9, and TM13 and TM14. The two discontinuous helices observed previously[11] are TM7 and TM12. They are interrupted in the middle of the bilayer by an extended loop of 5–7 residues. The tips of these loops contain a proline that is conserved between all three antiporter-like subunits: M(Pro 239)* in TM7 and M(Pro 399)* in TM12 (the prefix indicates the subunit name; asterisks indicate residues conserved between all three antiporter-like subunits). As in other transporters[22,23], such helices are likely to participate in proton or ion transport by introducing some flexibility and charge to the middle of the membrane.

TMs 1, 2 and 14 form a lipid-facing layer at the opposite side of the domain from helix HL and are the least conserved in sequence and in structure (Supplementary Figs 3 and 5). TMs 2 and 3 are connected at the periplasmic surface by an extended β-hairpin. The core of the subunits is formed by the well-conserved helices 4–13. Their arrangement has internal symmetry: TMs 4–8 can be superimposed on TMs 9–13 by a rotation of about 180° along the axis lying in the membrane plane and directed along the long axis of the domain, followed by a shift along this axis (Fig. 2c–f and Supplementary Movie 2). Thus, the two halves of the core, each containing five TMs, are related, uniquely, by symmetry along a pseudo-two-fold screw axis. Symmetry-related sets of helices in transporters may span the membrane in a parallel or antiparallel fashion, but have always been found in face-to-face arrangements, with substrate binding sites located near the symmetry axis at the domain interface[22]. However, in case of complex I antiporter-like subunits, the interface is formed by face-to-back contact, presenting a novel arrangement of symmetry-related helices. This places discontinuous helices 7 and 12 far apart, so that they cannot interact directly, in contrast to the situation in other transporters. It is likely that antiporter-like subunits have evolved by gene duplication[22], even though the sequences of the two inverted domains (Fig. 2c–e) have diverged (Supplementary Table 3).

At the centre of each antiporter-like subunit, TM8 is partly unwound in the middle and contains a kink with no proline residues, similar to the π-bulge in bacteriorhodopsin[24]. The secondary structure is markedly disrupted near the kink (residues L(253–258), M(259–264) and N(242–247)), indicating flexibility. Such π-bulges (or π-helices[25]) are normally found at protein functional sites[25], indicating a mechanistic importance for the kink in TM8.

Two well-studied, essential charged residues that are conserved from Mrp antiporters to complex I (refs 15, 26) are found in the middle of TM5 (L(Glu 144), M(Glu 144) and N(Glu 133); termed Glu TM5 here), and in the middle of TM7 (L(Lys 229), M(Lys 234) and N(Lys 217); Lys TM7). Lys TM7 is the last residue of the periplasmic half of discontinuous TM7 (TM7a), and its ε-amino group points inside the putative proton channel (termed here the first channel), formed by TMs 5–8. Notably, Glu TM5 is wedged at the interface of TMs 5 and 6, and is exposed both to this channel and to the cavity at the interface with the adjacent subunit. The Glu TM5 carboxyl group can interact electrostatically with the Lys TM7 amino group, which is about 5–6 Å away. An invariant Trp from TM7b (M(Trp 243)*) stabilizes the link between the two halves of TM7. The negative helix-dipole charge here may be partly compensated by N(Trp 247), M(His 248) and L(His 254).

The area near the second discontinuous helix, TM12, harbours many conserved polar residues in the middle of the membrane, so is also of clear functional importance. In NuoL and NuoN, an invariant, essential[27,28] lysine (L(Lys 399) and N(Lys 395)) lies at the beginning of the periplasmic half of TM12 (TM12b) in a position approximately symmetrical to Lys TM7 (Fig. 2d, e). It may interact with, and stabilize, the negatively charged C terminus of TM12a. In NuoM, a similar position is occupied by an invariant Glu 407. Here, the negative dipole moment may be stabilized by the invariant His 322. Notably, Glu 407 is replaced by an invariant lysine in the homologous MrpD subunit of antiporters. The side chain of this Lys or Glu (termed Lys/Glu TM12) is exposed in a large cavity between TMs 10–13. Thus, unexpectedly, a second putative proton channel is present here, related by inverted

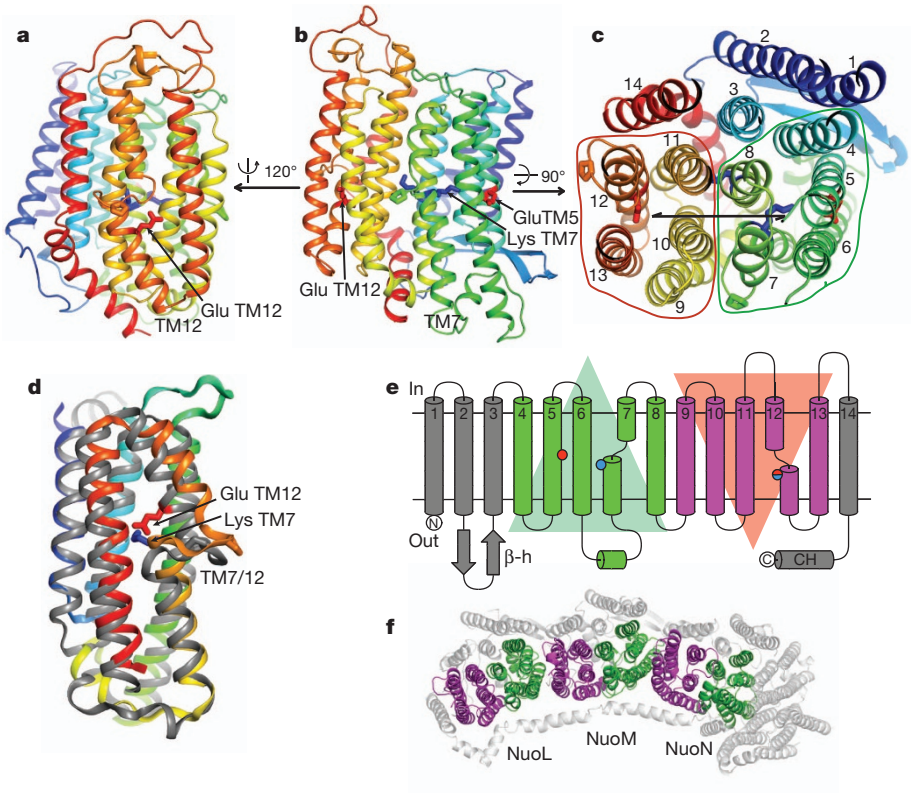

Figure 2 | Fold of antiporter-like subunits. The fold is illustrated using subunit NuoM. **a**, Side view, cytoplasmic side up, centred on TM12. **b**, Side view centred on TM7, coloured blue to red from N to C terminus. Essential charged residues are shown as sticks (Glu TM5 and Lys TM7 from channel 1, Glu TM12 from channel 2 and the connecting M(Lys 265) from TM8). Conserved prolines from intra-helical loops are also shown. **c**, View from the cytoplasm into the membrane. TM helices are numbered. Two inverted repeats are circled and the pseudo-two-fold symmetry screw axis that relates them is shown. **d**, Overlay of the two symmetry-related domains (TMs 9–13, in grey, over TMs 4–8). **e**, Topology diagram of antiporter-like subunits. Two inverted repeats of the conserved core are shown in green and magenta. Crucial charged residues (Glu TM5, Lys TM7 and Lys/Glu TM12) are indicated. **f**, Structural repeats in the membrane domain, seen from the cytoplasm. TMs 4–8 are highlighted in green and TMs 9–13, in magenta.

symmetry to the first channel. Additionally, N(Lys 395) is exposed to the cavity between NuoN and NuoM, and M(Glu 407) is partially exposed to the cavity between NuoM and NuoL, similarly to Glu TM5.

Searches using either complete subunits or the repeating domain revealed no structural analogues in the protein data bank (PDB), confirming that the fold is novel. Homologous subunits in Mrp antiporters, chloroplast Ndh complexes and membrane-bound hydrogenases, not yet structurally characterized, are likely to share the same core fold.

Fold of subunits NuoK, NuoJ and NuoA

In contrast to NuoL, M and N, the smaller subunits interact extensively, with large surface areas buried at interfaces. They also form more hydrogen bonds and salt bridges to their neighbours (Supplementary Table 4), 'gluing' together this end of the membrane domain.

NuoK spans the membrane with three linearly arranged α-helices, connected by short loops (Supplementary Fig. 6a). NuoK interacts extensively with NuoN (Fig. 1b), consistent with the presence of the analogous MrpC subunit in antiporters[29]. The C terminus of NuoK extends between helix HL and NuoN, forming many inter-subunit links. NuoK can be aligned with TMs 4–6 of antiporter-like subunits (and also with TMs 9–11, but with low sequence identities) (Supplementary Table 3). Notably, conserved K(Glu 36) aligns to Glu TM5, indicating that NuoK and the antiporter-like subunits might share an ancestor.

Subunit NuoJ has an unusual non-globular fold: three linearly arranged amino-terminal TM helices border NuoK, and TMs 4 and 5 are separated at the opposite sides of the domain (Supplementary Fig. 6b). Thus, NuoJ interweaves between NuoK, A and N, stabilizing the complex. TM3 of NuoJ contains in its middle a π-bulge/kink (residues 59–62), similar to TM8 in NuoL, M and N, so this helix is probably flexible and mechanistically important.

Subunit NuoA consists of three linearly arranged TM helices at the edge of the domain, interacting with NuoJ, N and K (Supplementary Fig. 6c). Its outer surface, including the conserved A(Asp 79) in the middle of the membrane, probably interacts with NuoH (Fig. 1c). A conserved loop between TM1 and TM2 is not resolved in the structure and probably interacts with the hydrophilic subunit NuoD[11]. The probable quinone-binding site is formed at the interface of subunits NuoH, J and A with the hydrophilic domain[11] (Fig. 1c).

Interactions between subunits

About half of the total subunit surface area is buried away from the solvent (Supplementary Table 4), consistent with the relative stability of the domain. However, interactions between antiporter-like subunits are not extensive. They mainly involve two helices from each subunit (TM5 and 6 and TM12 and 13), and are mostly hydrophobic, with very few hydrogen bonds (Supplementary Table 4). Crevices between subunits are likely to be filled with lipids, some of which are ordered and modelled here.

Helix HL stabilizes the complex. It is tightly anchored to NuoN, J and K by L(TM16), which also contacts N(TM7). HL contacts NuoM near M(TM7), where HL is unwound, allowing for strong interactions via the backbone and side chains (Fig. 3 and Supplementary Table 4). In a similar fashion, helix HL forms hydrogen bonds to the main body of the domain near TM7 of NuoL and N. These contacts involve conserved M(Lys 173)*, M(Asp 246)* and M(Tyr 317)*, and a semi-conserved residue, M(His 241).

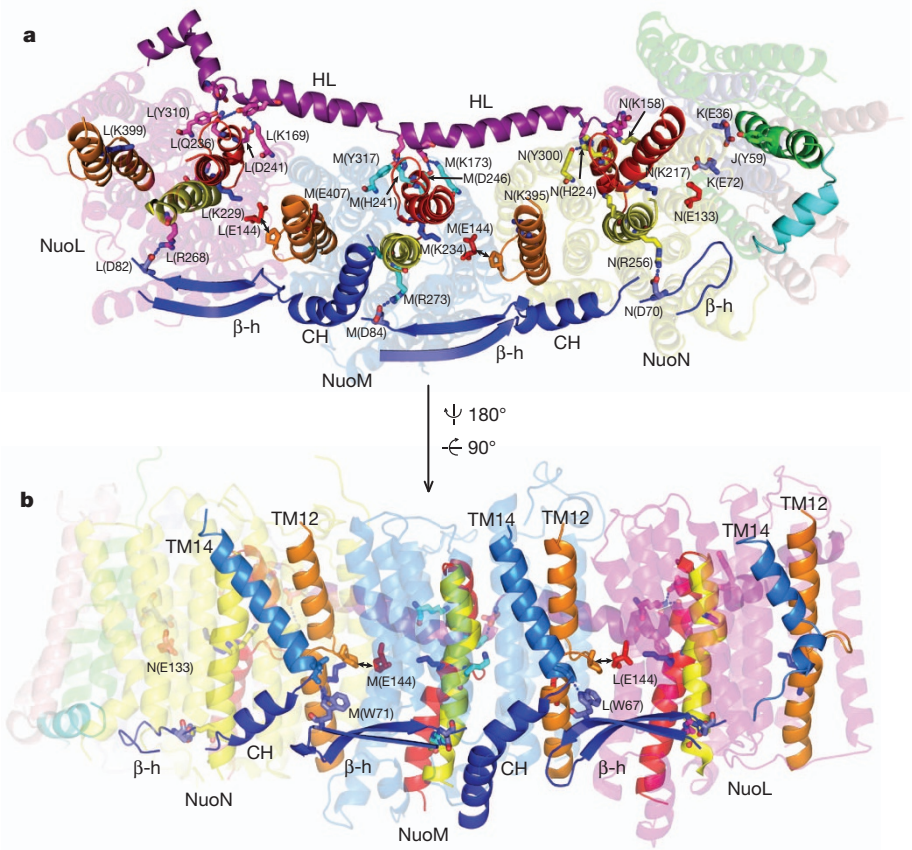

Figure 3 | Connecting elements and interactions between subunits. **a**, View from the periplasm. Helix HL is in purple and the β-hairpin-helix element βH (consisting of hairpins β-h and helices CH) is in blue. The contacting helix from NuoJ (preceding TM5 of NuoJ) is in cyan. Helices that are probably involved in conformational changes are shown in red (TM7 in NuoL, M and N), orange (TM12), yellow (TM8) and green (TM3 in NuoJ). Essential charged residues are shown as sticks and labelled (prefix indicates subunit). Also shown are conserved residues involved in contacts between antiporter-like subunits and helix HL, as well as between the β-hairpins and TM8. Putative hydrogen bonds are indicated. Potential interactions between Glu TM5 and a conserved proline from the TM12 loop are indicated by arrows. **b**, View in the membrane, with TM14 also shown (light blue). Tryptophan residues forming hydrogen bonds to the backbone at the C terminus of TM14 are indicated.

Notably, an additional element connecting antiporter-like subunits is present on the opposite side of the domain from helix HL. The extended and well-ordered (thus probably rigid) β-hairpins from neighbouring subunits contact each other via a stretch of C-terminal amphipathic helices termed CH (Fig. 3). This notable β-hairpin-helix element (termed the βH element) extends over the entire length of the antiporter-like subunits and contributes to the stability of the complex, because the only polar interactions between NuoM and NuoN are via the tip of the NuoM β-hairpin (there are also similar interactions between NuoM and NuoL; Supplementary Table 4). Predictions of secondary structure indicate that there are β-strands of similar length between TMs 2 and 3 in most other species, so the β-hairpin and second connecting element are likely to be common features.

Proton translocation pathways in subunits NuoL, M and N

The central positions of Lys TM7 and Lys TM12 in both channels, close to the breaks in TM7 and TM12, and the severe effects of their mutations (Supplementary Table 6), indicate that in complex I, unusually, lysine rather than carboxylate residues have a central role in the proton pump (one exception is M(Glu 407)). Examination of potential pathways (Supplementary Discussion, section 1) shows that none of the channels is solvent-accessible on both sides of the membrane.

In the first channel, the cavity surrounding Lys TM7 is about 70 Å^3 and is lined by 2–5 polar residues (Fig. 4a–c and Supplementary Table 5). It is closed from the periplasm by large hydrophobic residues but is open to the cytoplasm via a network of polar residues. Cavities between subunits L and M, and M and N, are blocked from the periplasm but may be accessible from the cytoplasm, possibly allowing an additional (but less likely; Supplementary Discussion, section 1) protonation route for Lys TM7, by 'side-entry' near Glu TM5.

The cavity in the second channel, near Lys/Glu TM12, is markedly larger and more hydrophilic than that in the first one (up to 200 Å^3, ~10 polar residues; Fig. 4a–c and Supplementary Table 5). Access to the cytoplasm is closed but the periplasm is accessible via short polar networks.

Many conserved charged and polar residues in the middle of the membrane connect the two channels in each subunit (Fig. 4, Supplementary Fig. 8 and Supplementary Table 5). Notably, in NuoM and NuoN, central positions in this connection are occupied by invariant essential residues[28,30,31] N(Lys 247) and M(Lys 265), found near the TM8 π-bulge. NuoL also contains an invariant residue, His 254, near this position.

Thus, in all antiporter-like subunits, unusually, two half-closed symmetry-related channels are linked, forming a single continuous proton translocation pathway through each subunit. Consistently, all the observed water molecules are either in the channels or in the connection (Fig. 4). Other pathways seem to be unlikely (Supplementary Discussion, section 2).

The fourth proton translocation pathway

An additional channel is apparent at the interface of subunits NuoN, K, J and A. A cavity of ~130 Å^3 between NuoN and NuoK can accommodate water molecules coordinated by K(Glu 72), N(Thr 160) and N(Ser 156)

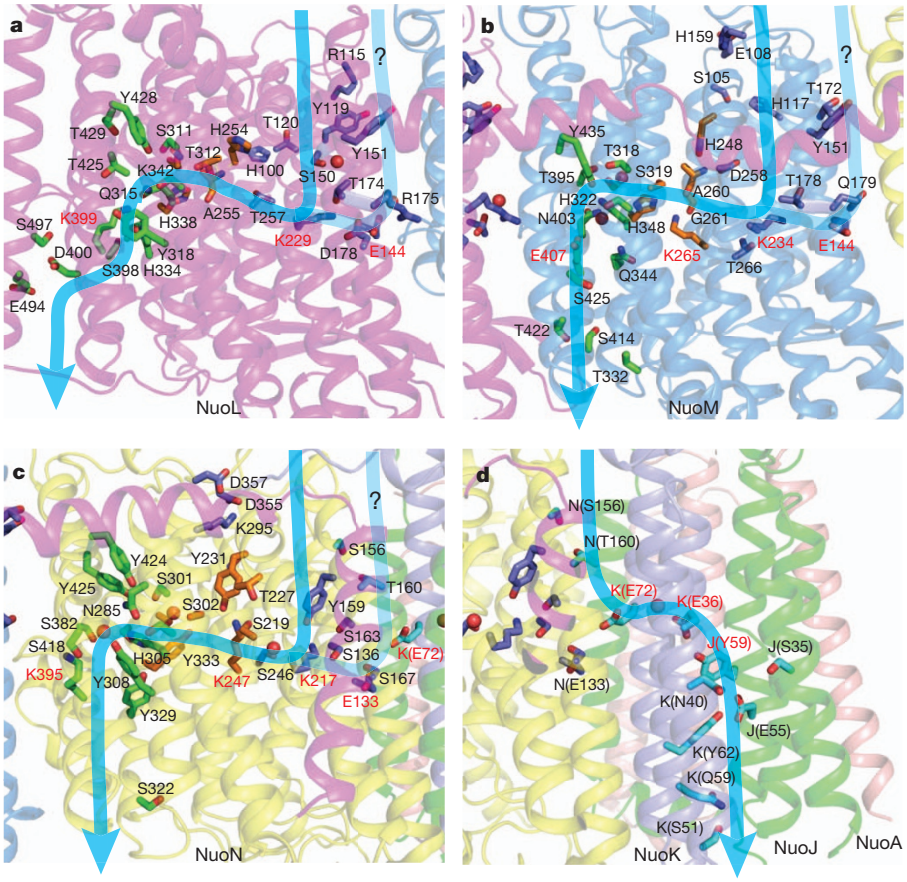

Figure 4 | Proton translocation channels. **a**–**c**, Putative channels in the antiporter-like subunits. Polar residues lining the channels are shown as sticks, with carbon in dark blue for the first channel, in green for the second channel and in orange for connecting residues. **d**, Channel at the interface of subunits NuoN, K and J, with polar residues in cyan. All views are in a similar orientation to Fig. 1a. Approximate proton translocation paths are indicated by blue arrows. Additional, less likely, input channels at the interfaces of subunits are paler in colour and labelled '?'. Essential charged residues are labelled in red. Water molecules resolved in the structure are shown as red spheres. Alanine and glycine from the π-bulge in TM8 may coordinate water molecules via exposed backbone carbonyls.

(Fig. 4d). Space for the cavity is provided by an invariant residue, K(Gly 76). Access to the periplasm is blocked by large hydrophobic residues but the cytoplasm is accessible with only a short constriction near K(Leu 83). Indeed, the structure shows a water molecule in the middle of the bilayer, between the conserved, essential residues[32,33] K(Glu 36) and K(Glu 72). From K(Glu 36), the continuation of the pathway is apparent at the interface of TMs 2 and 3 from NuoK and NuoJ, reaching the periplasm. Several small cavities here may contain water molecules coordinated by conserved polar residues (Fig. 4d). An alternative 'sideways' pathway from K(Glu 36) to the periplasm through invariant A(Glu 81) to A(Glu 102) can be considered, but is less likely, requiring a more extended network of water molecules.

Mechanism of proton translocation

There is no evidence in the structure for any potential electron carriers in the membrane domain, for the existence of quinone-binding sites in antiporter-like subunits, or for a different role of NuoN (Supplementary Discussion, section 4), as has been discussed in the literature[34–36]. Structural features combine to indicate strongly that complex I operates purely by a conformation-driven mechanism.

Conformational changes in the hydrophilic domain, which occur upon reduction[13], can be transmitted to the membrane-domain subunits NuoH, A, J and K (Supplementary Discussion, section 3). Helix HL can relay these changes to TM7 in NuoL, M and N, leading to protonation of Lys TM7 upon closer approach of Glu TM5. Recent studies have confirmed the essential coupling role of this helix[37,38] (Supplementary Discussion, section 4).

The structure indicates that conformational changes in both half-channels of the antiporter-like subunits are coordinated not only by helix HL, but by several connecting elements, acting in concert to achieve tight coupling of proton translocation events. HL can drive TM7 in the first channel, and, on the opposite side of the domain, the βH element can drive TM12 in the second channel. The two channels can interact both within subunits (via TM8, which contains an invariant connecting Lys or His near its flexible kink) and also between subunits, because the intra-helical loop of TM12 is in close contact with Glu TM5 on the neighbouring subunit. Furthermore, Glu TM5 can also interact electrostatically with Lys/Glu TM12 from a neighbouring subunit, because both residues are exposed to the inter-subunit cavities.

We suggest the following translocation cycle via antiporter-like subunits (Fig. 5), assuming that Lys TM7 is protonated and that Lys/Glu TM12 is deprotonated in the oxidized state (meaning the state of iron-sulphur cluster N2 and a nearby cluster[13], because most clusters are reduced during turnover[39]). Conformational changes upon reduction move Glu TM5 away from Lys TM7, forcing lysine to donate its proton into the link between the two half-channels and eventually to Lys/Glu TM12, which becomes protonated owing to local conformational changes, either with or without help from Glu TM5 from the neighbouring subunit. Upon return to the oxidised-state conformation, Glu TM5 moves back, Lys TM7 is protonated from the cytoplasm, reloading the pump, and Lys/Glu TM12 ejects its proton into the periplasm. Overall, three subunits translocate three protons.

In the fourth putative channel, a notable feature indicating conformational coupling is the π-bulge on TM3 of NuoJ, which contains a

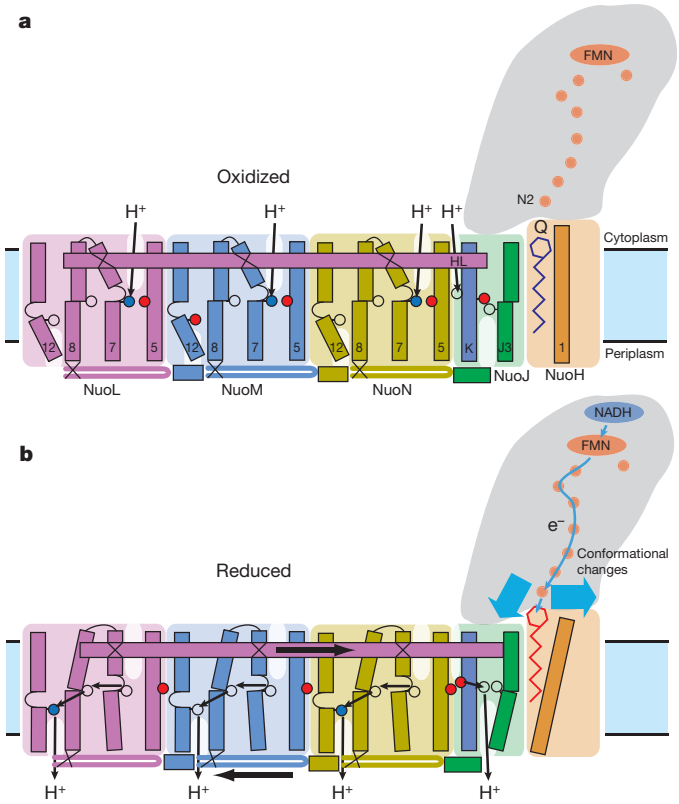

Figure 5 | Proposed mechanism of complex I. **a**, Oxidised state. **b**, Reduced state. Conformational coupling between electron transfer and proton translocation is mediated by helix HL (cytoplasmic side) and the βH element (periplasmic side). TM helices are numbered. Crucial charged residues (Glu TM5, Lys TM7, Lys/Glu TM12 and Lys/His TM8 from NuoL, M and N, as well as K(Glu 72) and K(Glu 36), interacting with J(Tyr 59)) are indicated by red or empty circles (Glu) and empty or blue circles (Lys) for unprotonated or protonated residues, respectively. In NuoL, M and N, Lys TM7 from the first half-channel is assumed to be protonated in the oxidized state. Upon reduction, it donates its proton to the connecting Lys/His TM8 and then on to Lys/Glu TM12 from the second half-channel. Lys/Glu TM12 ejects its proton into periplasm upon return from the reduced to the oxidized state. A fourth proton per cycle is translocated at the interface of NuoN, K and J.

residue that is invariant and important for activity[40,41], J(Tyr 59), forming a hydrogen bond to K(Glu 36), a central residue of this channel. TM3 is the most conserved helix in NuoJ (Supplementary Figs 3a and 8) and is a hotspot for human mitochondrial disease mutations (Supplementary Table 7). Conformational changes, propagating from the nearby hydrophilic domain, can move the flexible TM3 of NuoJ and J(Tyr 59), resulting in the protonation/deprotonation of K(Glu 36) and the translocation of the fourth proton (Fig. 5). Because the four channels that are present in the structure account for the measured H^+/e^- stoichiometry[42], any additional direct coupling, as proposed recently[43,44], is unlikely.

Our knowledge of the structure of the core subunits of complex I is now nearly complete (except for subunit NuoH). The effects of many mutations, including those causing human diseases, can now be understood (Supplementary Tables 6–8). This molecular machine has one of the most intricate architectures among known protein structures. The redox energy of NADH, binding at the tip of the hydrophilic domain, is eventually used in the membrane domain, at distances of up to ~300 Å away. Our previously published analogy of the 'steam engine of the cell' is emphasized by the presence of several connecting elements, including helix HL, which are powered by the redox energy of electron transfer and which drive six symmetrical structural domains, plus one asymmetrical domain, resulting in a very effective proton pump.

METHODS SUMMARY

The membrane domain of *E.coli* complex I was purified as previously described[11], except that the detergent cymal-7 was used. Protein was crystallized in the presence of lipids using polyethylene glycol (PEG) 4000 and sodium tartrate as the precipitant at pH 4.8, with the additives 0.15% sodium cholate and 0.1 M NDSB-256 (non detergent sulfobetaine-256). Diffraction was improved by a slow increase of PEG 4000 concentration to 30%, by dialysis at 4 °C.

Diffraction data were collected from cryo-cooled crystals (100 K) on beamline ID29 at the European Synchrotron Radiation Facility (ESRF) and X06SA at the Swiss Light Source (SLS). Crystallographic phases were obtained using selenomethionine-labelled protein. Electron density was improved by multi-crystal averaging and density modification. The folds of individual subunits and sequence register at the initial steps of model building were determined using the positions of anomalous density peaks from Se atoms, directionality of helices and density connectivity. A combination of manual and automatic model building was used. Data collection and refinement statistics are presented in Supplementary Table 1.

Full Methods and any associated references are available in the online version of the paper at www.nature.com/nature.

Received 2 March; accepted 24 June 2011.
Published online 7 August 2011.

1. Walker, J. E. The NADH:ubiquinone oxidoreductase (complex I) of respiratory chains. *Q. Rev. Biophys.* **25,** 253–324 (1992).
2. Yagi, T. & Matsuno-Yagi, A. The proton-translocating NADH–quinone oxidoreductase in the respiratory chain: the secret unlocked. *Biochemistry* **42,** 2266–2274 (2003).
3. Brandt, U. Energy converting NADH:quinone oxidoreductase (complex I). *Annu. Rev. Biochem.* **75,** 69–92 (2006).
4. Ohnishi, T. Iron-sulfur clusters/semiquinones in complex I. *Biochim. Biophys. Acta* **1364,** 186–206 (1998).
5. Sazanov, L. A. Respiratory complex I: mechanistic and structural insights provided by the crystal structure of the hydrophilic domain. *Biochemistry* **46,** 2275–2288 (2007).
6. Schapira, A. H. Human complex I defects in neurodegenerative diseases. *Biochim. Biophys. Acta* **1364,** 261–270 (1998).
7. Dawson, T. M. & Dawson, V. L. Molecular pathways of neurodegeneration in Parkinson's disease. *Science* **302,** 819–822 (2003).
8. Balaban, R. S., Nemoto, S. & Finkel, T. Mitochondria, oxidants, and aging. *Cell* **120,** 483–495 (2005).
9. Carroll, J. *et al.* Bovine complex I is a complex of 45 different subunits. *J. Biol. Chem.* **281,** 32724–32727 (2006).
10. Yip, C. Y., Harbour, M. E., Jayawardena, K., Fearnley, I. M. & Sazanov, L. A. Evolution of respiratory complex I: "supernumerary" subunits are present in the alpha-proteobacterial enzyme. *J. Biol. Chem.* **286,** 5023–5033 (2011).
11. Efremov, R. G., Baradaran, R. & Sazanov, L. A. The architecture of respiratory complex I. *Nature* **465,** 441–445 (2010).
12. Sazanov, L. A. & Hinchliffe, P. Structure of the hydrophilic domain of respiratory complex I from *Thermus thermophilus*. *Science* **311,** 1430–1436 (2006).
13. Berrisford, J. M. & Sazanov, L. A. Structural basis for the mechanism of respiratory complex I. *J. Biol. Chem.* **284,** 29773–29783 (2009).
14. Fearnley, I. M. & Walker, J. E. Conservation of sequences of subunits of mitochondrial complex I and their relationships with other proteins. *Biochim. Biophys. Acta* **1140,** 105–134 (1992).
15. Mathiesen, C. & Hagerhall, C. Transmembrane topology of the NuoL, M and N subunits of NADH:quinone oxidoreductase and their homologues among membrane-bound hydrogenases and bona fide antiporters. *Biochim. Biophys. Acta* **1556,** 121–132 (2002).
16. Friedrich, T. Complex I: a chimaera of a redox and conformation-driven proton pump? *J. Bioenerg. Biomembr.* **33,** 169–177 (2001).
17. Hunte, C., Zickermann, V. & Brandt, U. Functional modules and structural basis of conformational coupling in mitochondrial complex I. *Science* **329,** 448–451 (2010).
18. Baranova, E. A., Holt, P. J. & Sazanov, L. A. Projection structure of the membrane domain of *Escherichia coli* respiratory complex I at 8 Å resolution. *J. Mol. Biol.* **366,** 140–154 (2007).
19. von Heijne, G. Membrane protein structure prediction. Hydrophobicity analysis and the positive-inside rule. *J. Mol. Biol.* **225,** 487–494 (1992).
20. Yau, W. M., Wimley, W. C., Gawrisch, K. & White, S. H. The preference of tryptophan for membrane interfaces. *Biochemistry* **37,** 14713–14718 (1998).
21. Vik, S. B. The transmembrane helices of the L, M, and N subunits of Complex I from *E. coli* can be assigned on the basis of conservation and hydrophobic moment analysis. *FEBS Lett.* **585,** 1180–1184 (2011).
22. Vinothkumar, K. R. & Henderson, R. Structures of membrane proteins. *Q. Rev. Biophys.* **43,** 65–158 (2010).
23. Screpanti, E. & Hunte, C. Discontinuous membrane helices in transport proteins and their correlation with function. *J. Struct. Biol.* **159,** 261–267 (2007).
24. Luecke, H., Schobert, B., Richter, H. T., Cartailler, J. P. & Lanyi, J. K. Structure of bacteriorhodopsin at 1.55 Å resolution. *J. Mol. Biol.* **291,** 899–911 (1999).
25. Cooley, R. B., Arp, D. J. & Karplus, P. A. Evolutionary origin of a secondary structure: π-helices as cryptic but widespread insertional variations of α-helices that enhance protein functionality. *J. Mol. Biol.* **404,** 232–246 (2010).

26. Morino, M. *et al.* Single site mutations in the hetero-oligomeric Mrp antiporter from alkaliphilic *Bacillus pseudofirmus* OF4 that affect Na^+/H^+ antiport activity, sodium exclusion, individual Mrp protein levels, or Mrp complex formation. *J. Biol. Chem.* **285,** 30942–30950 (2010).
27. Nakamaru-Ogiso, E. *et al.* the membrane subunit NuoL (ND5) is involved in the indirect proton pumping mechanism of *Escherichia coli* complex I. *J. Biol. Chem.* **285,** 39070–39078 (2010).
28. Amarneh, B. & Vik, S. B. Mutagenesis of subunit N of the *Escherichia coli* complex I. Identification of the initiation codon and the sensitivity of mutants to decylubiquinone. *Biochemistry* **42,** 4800–4808 (2003).
29. Mathiesen, C. & Hagerhall, C. The 'antiporter module' of respiratory chain complex I includes the MrpC/NuoK subunit—a revision of the modular evolution scheme. *FEBS Lett.* **549,** 7–13 (2003).
30. Euro, L., Belevich, G., Verkhovsky, M. I., Wikstrom, M. & Verkhovskaya, M. Conserved lysine residues of the membrane subunit NuoM are involved in energy conversion by the proton-pumping NADH:ubiquinone oxidoreductase (complex I). *Biochim. Biophys. Acta* **1777,** 1166–1172 (2008).
31. Torres-Bacete, J., Nakamaru-Ogiso, E., Matsuno-Yagi, A. & Yagi, T. Characterization of the NuoM (ND4) subunit in *Escherichia coli* NDH-1: conserved charged residues essential for energy-coupled activities. *J. Biol. Chem.* **282,** 36914–36922 (2007).
32. Kao, M. C., Nakamaru-Ogiso, E., Matsuno-Yagi, A. & Yagi, T. Characterization of the membrane domain subunit NuoK (ND4L) of the NADH-quinone oxidoreductase from *Escherichia coli. Biochemistry* **44,** 9545–9554 (2005).
33. Kervinen, M., Patsi, J., Finel, M. & Hassinen, I. E. A pair of membrane-embedded acidic residues in the NuoK subunit of *Escherichia coli* NDH-1, a counterpart of the ND4L subunit of the mitochondrial complex I, are required for high ubiquinone reductase activity. *Biochemistry* **43,** 773–781 (2004).
34. Fisher, N. & Rich, P. R. A motif for quinone binding sites in respiratory and photosynthetic systems. *J. Mol. Biol.* **296,** 1153–1162 (2000).
35. Ohnishi, T., Nakamaru-Ogiso, E. & Ohnishi, S. T. A new hypothesis on the simultaneous direct and indirect proton pump mechanisms in NADH-quinone oxidoreductase (complex I). *FEBS Lett.* **584,** 4131–4137 (2010).
36. Nakamaru-Ogiso, E., Sakamoto, K., Matsuno-Yagi, A., Miyoshi, H. & Yagi, T. The ND5 subunit was labeled by a photoaffinity analogue of fenpyroximate in bovine mitochondrial complex I. *Biochemistry* **42,** 746–754 (2003).
37. Steimle, S. *et al.* The role of subunit NuoL for proton translocation by the respiratory complex I. *Biochemistry* **50,** 3386–3393 (2011).
38. Michel, J., Deleon-Rangel, J., Zhu, S., Van Ree, K. & Vik, S. B. mutagenesis of the L, M, and N subunits of complex I from *Escherichia coli* indicates a common role in function. *PLoS ONE* **6,** e17420 (2011).
39. Krishnamoorthy, G. & Hinkle, P. C. Studies on the electron transfer pathway, topography of iron-sulfur centers, and site of coupling in NADH-Q oxidoreductase. *J. Biol. Chem.* **263,** 17566–17575 (1988).
40. Kao, M. C. *et al.* Characterization of the membrane domain subunit NuoJ (ND6) of the NADH-quinone oxidoreductase from *Escherichia coli* by chromosomal DNA manipulation. *Biochemistry* **44,** 3562–3571 (2005).
41. Pätsi, J., Kervinen, M., Finel, M. & Hassinen, I. E. Leber hereditary optic neuropathy mutations in the ND6 subunit of mitochondrial complex I affect ubiquinone reduction kinetics in a bacterial model of the enzyme. *Biochem. J.* **409,** 129–137 (2008).
42. Galkin, A. S., Grivennikova, V. G. & Vinogradov, A. D. $H^+/2e^-$ stoichiometry in NADH-quinone reductase reactions catalyzed by bovine heart submitochondrial particles. *FEBS Lett.* **451,** 157–161 (1999).
43. Treberg, J. R. & Brand, M. D. A model of the proton translocation mechanism of complex I. *J. Biol. Chem.* **286,** 17579–17584 (2011).
44. Ohnishi, S. T., Salerno, J. C. & Ohnishi, T. Possible roles of two quinone molecules in direct and indirect proton pumps of bovine heart NADH-quinone oxidoreductase (complex I). *Biochim. Biophys. Acta* **1797,** 1891–1893 (2010).

Supplementary Information is linked to the online version of the paper at www.nature.com/nature.

Acknowledgements This work was funded by the Medical Research Council. We thank the ESRF and the SLS for provision of synchrotron radiation facilities. We are grateful to the staff of beamlines ID29 (ESRF) and X06SA (SLS) for assistance.

Author Contributions R.G.E. performed research and analysed data; L.A.S. designed the project, analysed data and wrote the manuscript, with contributions from R.G.E.

Author Information The coordinates and structure factors have been deposited in the RCSB Protein Data Bank under accession code 3RKO. Reprints and permissions information is available at www.nature.com/reprints. The authors declare no competing financial interests. Readers are welcome to comment on the online version of this article at www.nature.com/nature. Correspondence and requests for materials should be addressed to L.A.S. (sazanov@mrc-mbu.cam.ac.uk).

METHODS

Protein purification, crystallization and post-crystallization treatment. Complex I from *E. coli* was purified from strain BL21(DE3) as previously described[45]. The membrane and hydrophilic domains were separated[11] by treatment with a high concentration of Mg^{2+}: purified complex I (2.5 mg ml^{-1}) was incubated in 20 mM Bis-Tris (pH 6.0), 5% (v/v) glycerol, 400 mM $MgCl_2$, 12.5 mM NaCl, 0.5 mM $CaCl_2$ and 0.25% (w/v) *n*-dodecyl-β-maltoside (Glycon) for 2 h on ice. The protein solution was diluted tenfold with buffer A (20 mM Bis-Tris (pH 6.0), 0.02% cymal-7 (Anatrace)), loaded onto a Mono-S HR 5/5 column and eluted with a 25 ml gradient, from 10% to 70%, of buffer B (1 M NaCl in buffer A). Fractions containing the membrane arm were pooled, concentrated in 100-kDa MWCO concentrators (Ultracel-100K, Amicon), diluted tenfold with 10 mM sodium acetate (pH 4.8), 50 mM NaCl and 0.02% cymal-7, and concentrated to 10–11 mg ml^{-1}.

Before crystallization, lipids (1,2-dimyristoleoyl-*sn*-glycerol-3-phosphocholine with *E. coli* polar lipids at a 3:1 ratio (w/w), Avanti Polar Lipids) were added to the protein to 2 mg ml^{-1} final concentration. Crystals were grown by the sitting drop method, mixing protein at 1:1 (v/v) ratio with 0.1 M sodium acetate (pH 4.8), 0.3 M sodium tartrate (pH 5.0), 9% (w/v) PEG 4000, 0.15% sodium cholate and either 0.1 M NDSB-256 or 0.4% nonyl-glucoside from Detergent Screen HT (Hampton Research). Crystals grew at 22 °C as thin plates of up to 200 μm in length and 20–40 μm in thickness. They were harvested after 3 weeks to 4 months, and initially diffracted to 7 Å resolution. To improve diffraction properties, crystals were slowly cooled to 4 °C, placed into micro-dialysis buttons, and mother liquor was exchanged by dialysis for 0.1 M sodium acetate (pH 4.8), 0.15 M sodium tartrate (pH 5.0), 30% PEG 4000, 0.1% sodium cholate and 12.5% glycerol over a period of 5 days.

For selenomethionine labelling, a feedback inhibition method[46] was applied during cell growth on M9-derived minimal media with 0.6% malate (optimized for maximal yield of complex I) as a carbon source. Purification and crystallization conditions were identical to those for native protein except for the addition of 10 mM tris(2-carboxyethyl)phosphine (TCEP, Thermo Scientific) to crystallization solutions.

Because the crystals were obtained at low pH and it is known that *E. coli* complex I dissociates into hydrophilic and hydrophobic domains after prolonged incubation at pH outside the 5.5–6.5 range[47], we assayed the purified enzyme for NADH:DQ activity at pH 4.8. The activity is lower than at optimal pH[45], but is still substantial (~4 μmol NADH oxidised per min per mg protein). It is still fully inhibited by piericidin A, indicating that enzyme is functional and that there are no drastic effects of pH on the conformation of the entire complex or individual domains.

Data collection and processing. Data were collected at 100 K with an ADSC Q210 detector at beamline ID29 at the European Synchrotron Radiation Facility and a Marmosaic 225 detector on the high-resolution diffractometer of beamline X06SA at the Swiss Light Source. Image data were processed with MOSFLM and SCALA from the CCP4 suite[48].

Model building and refinement. Crystals grew in space group *P*1 with two molecules in the unit cell and 70% solvent content. As is the case with orthorhombic crystals[11], triclinic crystals were non-isomorphous and diffracted anisotropically, with the worst diffraction along the *a* axis and comparable resolution along axes *b* and *c*; the *c* axis being systematically slightly better. Using the Diffraction Anisotropy Server (http://services.mbi.ucla.edu/anisoscale/)[49], the best native data set was anisotropically scaled and truncated to 3.4 Å, 3.0 Å and 3.0 Å resolution, where the F/σ ratio drops to ~2.6–2.8 along the a^*, b^* and c^* axes, respectively (scaling 2, Supplementary Table 1), resulting in better-quality electron density maps. As a control, the final model was also refined against non-truncated raw data at 3.2 Å resolution, with excellent statistics (scaling 1, Supplementary Table 1). Crystal packing resembles that observed previously in space group $P2_12_12_1$, with strong interactions between hydrophilic surfaces and no visible side contacts, explaining the weaker diffraction along the *a* axis (Supplementary Fig. 2). It is possible that side contacts are mediated by poorly ordered lipids.

Several anomalous diffraction data collected from selenomethionine-containing crystals were used for phasing (Supplementary Table 1). Despite challenges presented by anomalous data collection in the *P*1 space group, several good quality MAD data sets were obtained using a low-intensity beam and, in some cases, inverse-beam geometry. Initially, the positions of more than 140 Se atoms in the unit cell were determined and refined automatically in PHASER[50], using molecular replacement (MR) phases from the backbone model of the membrane fragment of *E. coli* complex I (PDB code 3M9C, ref. 11). The correspondence of the Se positions with peaks on the anomalous difference map was verified manually. When such maps were calculated with phases improved by density modification, the positions of 80 Se atoms per molecule were revealed. Experimental MAD phases calculated with these Se atoms in SHARP[51] gave a figure of merit of 0.23 in the resolution range between 20 Å and 3.5 Å, with the anomalous phasing power from peak, inflection and remote data sets being 0.608, 0.368 and 0.195, respectively. Isomorphous phasing power for inflection and remote data sets was 0.158 and 0.198, respectively. Phases were improved and extended by multi-crystal averaging with histogram matching and solvent flattening in the CCP4-suite program DMmulti. The molecular masks and transformation matrices were obtained from MR solutions. Four data sets were used: two from two *P*1 crystals (one native and one with Se MAD phases, Supplementary Table 1), and two phased data sets in the $P2_12_12_1$ space group from our previous study (Supplementary Table 1 in ref. 11, crystals Native1 with TaBr1 MAD phases and Native3 with TaBr3 SAD phases). Additionally, a solvent-flipped map was calculated in CNS[52] using MAD data from a single SeMet-containing crystal. The maps were of excellent quality; they had better connectivity in DMmulti maps and, occasionally, better side-chain density in CNS maps, so both maps were used during model building.

Individual subunit folds and sequence register at the initial steps of model building were deduced on the basis of Se atom positions, directionality of helices determined using the 'find_helices_strands' procedure in PHENIX[53], and local density averaging in O (ref. 54), as well as density connectivity. An initial model was built by combining manual building in O and Coot v.0.6.1 (ref. 55) with automatic model building in Buccaneer v.1.5 (ref. 56). The model was rebuilt manually during cycles of refinement. The structure was refined in PHENIX. A subset of 2% of structure factors was omitted from refinement and used for cross-validation (calculation of R_{free}). Simulated annealing was used in the early stages; secondary structure and non-crystallographic symmetry restraints were used throughout the refinement and TLS (translation, libration and screw-rotation displacements parametrization) was used during the final refinement. For initial refinement, Se MAD experimental or blurred phases from multi-crystal averaging were used, whereas final refinement was only against native data. Several well ordered internal water molecules were modelled on the basis of their well defined electron density, presence of coordinating residues and low B-factor upon refinement. The final model includes 1,952 residues, one cymal-7 molecule, eight water molecules and nine fragments of lipid aliphatic chains. The structure was validated in PROCHEK[57] and MOLPROBITY[58] and was found to be of better-than-average quality for the resolution. As calculated with PROCHEK, 87.0/12.3/0.3/0.0% of residues are in preferable/allowed/generously allowed/disallowed Ramachandran regions, respectively.

Bioinformatics. Searches for structural analogs in the PDB were performed using the SSM server (www.ebi.ac.uk/msd-srv/ssm/cgi-bin/ssmserver). In the case of NuoK and NuoA, as expected for small transmembrane proteins, similar folds could be found in the PDB, but without any significant sequence similarity. Structure-based multiple sequence alignments were performed in CLUSTALW v1.83 (ref. 59) with the profile alignment option. Homology models of the 14 conserved TM helices of Mrp subunits A and D from *Bacillus subtilis* and *Bacillus pseudofirmus* were built with MODELLER 9v7 (ref. 60) using structures of the *E. coli* subunits NuoL and NuoM, respectively, as templates. Sequences for modelling were aligned with CLUSTALW, using 30 sequences for NuoL or NuoM in addition to Mrp sequences and the structure-based profile alignment option. Figures were prepared in PyMol.

45. Sazanov, L. A., Carroll, J., Holt, P., Toime, L. & Fearnley, I. M. A role for native lipids in the stabilization and two-dimensional crystallization of the *Escherichia coli* NADH-ubiquinone oxidoreductase (Complex I). *J. Biol. Chem.* **278,** 19483–19491 (2003).
46. Van Duyne, G. D., Standaert, R. F., Karplus, P. A., Schreiber, S. L. & Clardy, J. Atomic structures of the human immunophilin FKBP-12 complexes with FK506 and rapamycin. *J. Mol. Biol.* **229,** 105–124 (1993).
47. Leif, H., Sled, V. D., Ohnishi, T., Weiss, H. & Friedrich, T. Isolation and characterization of the proton-translocating NADH: ubiquinone oxidoreductase from *Escherichia coli*. *Eur. J. Biochem.* **230,** 538–548 (1995).
48. Collaborative Computational Project 4. The CCP4 suite: programs for protein crystallography. *Acta Crystallogr. D* **50,** 760–763 (1994).
49. Strong, M. *et al.* Toward the structural genomics of complexes: crystal structure of a PE/PPE protein complex from *Mycobacterium tuberculosis*. *Proc. Natl Acad. Sci. USA* **103,** 8060–8065 (2006).
50. McCoy, A. J. *et al.* Phaser crystallographic software. *J. Appl. Cryst.* **40,** 658–674 (2007).
51. de La Fortelle, E. & Bricogne, G. Maximum-likelihood heavy-atom parameter refinement for multiple isomorphous replacement and multiwavelength anomalous diffraction methods. *Methods Enzymol.* **276,** 472–494 (1997).
52. Brunger, A. T. Version 1.2 of the crystallography and NMR system. *Nature Protocols* **2,** 2728–2733 (2007).
53. Adams, P. D. *et al.* PHENIX: building new software for automated crystallographic structure determination. *Acta Crystallogr. D* **58,** 1948–1954 (2002).
54. Jones, T. A. & Kjeldgaard, M. Electron-density map interpretation. *Methods Enzymol.* **277,** 173–208 (1997).
55. Emsley, P. & Cowtan, K. Coot: model-building tools for molecular graphics. *Acta Crystallogr.D* **60,** 2126–2132 (2004).
56. Cowtan, K. The Buccaneer software for automated model building. 1. Tracing protein chains. *Acta Crystallogr. D* **62,** 1002–1011 (2006).
57. Laskowski, R. A., MacArthur, M. W., Moss, D. S. & Thornton, J. M. PROCHECK: a program to check the stereochemical quality of protein structures. *J. Appl. Cryst.* **26,** 283–291 (1993).

58. Chen, V. B. *et al.* MolProbity: all-atom structure validation for macromolecular crystallography. *Acta Crystallogr. D* **66,** 12–21 (2010).
59. Thompson, J. D., Higgins, D. G. & Gibson, T. J. CLUSTAL W: improving the sensitivity of progressive multiple sequence alignment through sequence weighting, position-specific gap penalties and weight matrix choice. *Nucleic Acids Res.* **22,** 4673–4680 (1994).
60. Eswar, N. *et al.* Comparative protein structure modeling using Modeller. *Curr. Protoc. Bioinformatics* **Ch. 5**, Unit 5.6 (2006).